SUPPLEMENTARY MATERIAL

The goal of this supplementary material is to demonstrate that the simulation methodology used to study the physics of EIT is appropriate and provides accurate results. To do so, two codes using different numerics have been developed and compared. In addition, a mesh convergence analysis has been carried out to determine the size of the smallest physical scale that should be captured to properly simulate viscoelastic turbulence. This convergence analysis is also used to measure the effects of the spatial resolution on the solution.

In order to emphasize that our conclusions are also valid for more challenging cases, the flow conditions considered in this analysis slightly differ from those reported in the main paper. Specifically, a lower Reynolds number, $\mathrm{Re}_\tau = 40$, and a larger Weissenberg number, $\mathrm{Wi}_\tau = 310$, have been selected. This reduces the amount of inertia in the flow and thus amplifies the effects of polymer diffusion on the solution, while keeping a self-sustained EIT state. All the results reported in this supplementary material are obtained from two-dimensional simulations.

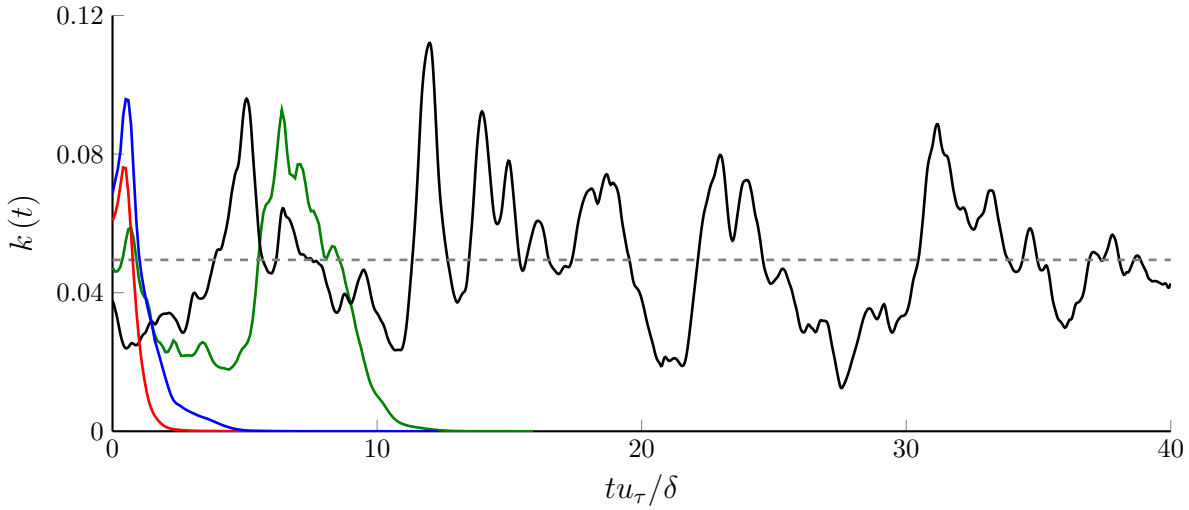

FIG. 1. Time series of the volume-averaged instantaneous turbulent kinetic energy $k\,(t)$ for $\mathrm{Re}_\tau = 40$, $\mathrm{Wi}_\tau = 310$ and different Schmidt numbers: $\mathrm{Sc} = 9$, $\mathrm{Sc} = 25$, $\mathrm{Sc} = 50$, $\mathrm{Sc} = 100$. The initial time, $t = 0$, is defined as the time when the blowing-suction perturbation is turned off.

Time series of the volume-averaged instantaneous turbulent kinetic energy $k\,(t)$ are reported in Figure 1 for different Schmidt numbers. The quantity $k\,(t)$ is defined as

$$k\,(t) = \left\langle \frac{1}{2}\frac{\mathbf{u}'\,(\mathbf{x},t)\cdot\mathbf{u}'\,(\mathbf{x},t)}{u_\tau^2} \right\rangle_\Omega \qquad \text{with} \qquad \mathbf{u}'\,(\mathbf{x},t) = \mathbf{u}\,(\mathbf{x},t) - \overline{\mathbf{u}\,(\mathbf{x},t)}\,, \tag{1}$$

where the spatial and time averaging operators,

$$\langle \bullet \rangle_\Omega = \frac{1}{\Omega}\int_\Omega \bullet \,\mathrm{d}\Omega \qquad \text{and} \qquad \bar{\bullet} = \frac{1}{T_s}\int_{t_0}^{t_0+T_s} \bullet \,\mathrm{d}t\,, \tag{2}$$

are introduced, Ω is the channel volume and T_s the sampling window for temporal averaging. The evolution of the turbulent kinetic energy shows that, for the present flow conditions, Sc has to be between 50 and 100 to allow EIT to sustain itself over time; large polymer diffusivity leads to flow laminarization. In this case, the critical Schmidt number above which a non-laminar state is sustained is larger than the one reported for $\mathrm{Re}_\tau = 85$, $\mathrm{Wi}_\tau = 40$ owing to the lower contribution of inertia at $\mathrm{Re}_\tau = 40$.

Each simulation reported in Figure 1 has been performed using a spatial resolution Δ that captures the viscous Batchelor scale, i.e., $\Delta \approx \eta_{\mathrm{B},\nu} = \delta_\nu \mathrm{Sc}^{-1/2} = \delta\ \mathrm{Re}_\tau^{-1}\mathrm{Sc}^{-1/2}$. Because (i) Batchelor theory only applies to a passive scalar, which is not the case in EIT, and (ii) EIT strongly differs from classical Newtonian turbulence, the pertinence of defining the mesh based on δ_ν and η_B is not *a priori* obvious. In order to verify *a posteriori* how the smallest physical scale compares to $\eta_{\mathrm{B},\nu}$, a mesh convergence analysis has been performed. The mean volume-averaged turbulent kinetic energy $\overline{k\,(t)}$ and mean volume-averaged polymer elongation mean square fluctuations $\left\langle \overline{C'^2\,(\mathbf{x},t)} \right\rangle_\Omega$ are reported in Figure 2 for different meshes, where $C'\,(\mathbf{x},t) = \mathrm{tr}\left(\mathbf{C}\,(\mathbf{x},t) - \overline{\mathbf{C}\,(\mathbf{x},t)}\right)/L^2$. The solution obtained for $\Delta \approx \eta_{\mathrm{B},\nu}$ (i.e.,

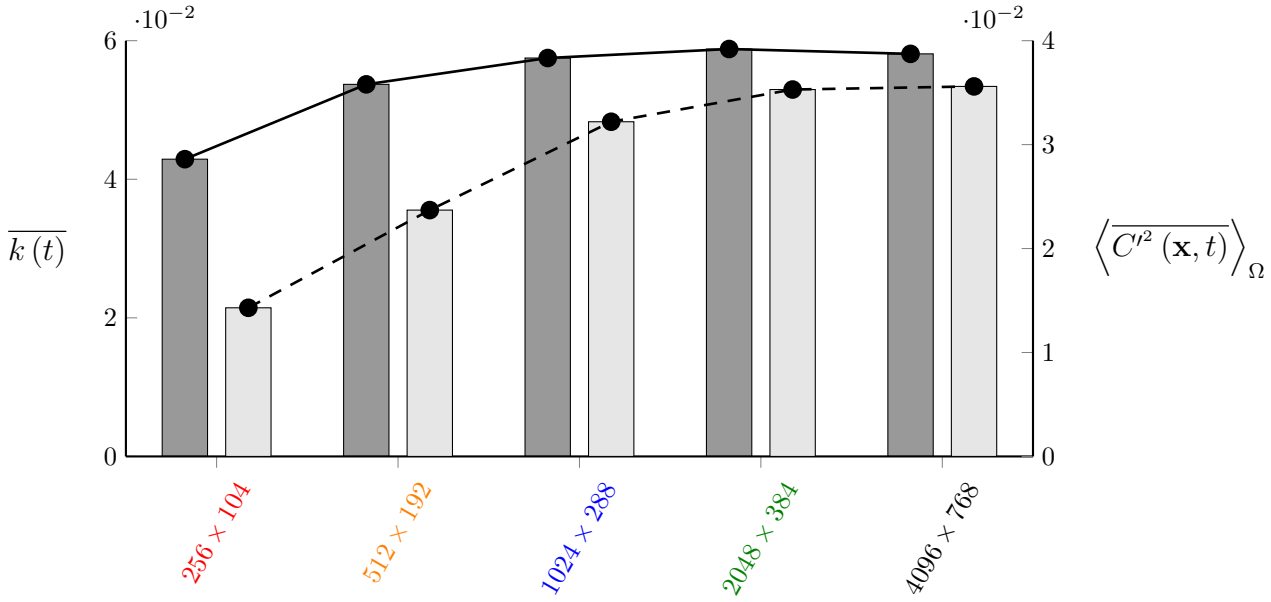

FIG. 2. Mean volume-averaged turbulent kinetic energy $\overline{k\,(t)}$ (dark gray bars, plain line, left y-axis) and mean volume-averaged polymer elongation mean square fluctuations $\left\langle \overline{C'^2\,(\mathbf{x},t)} \right\rangle_\Omega$ (light gray bars, dashed line, right y-axis) for $\mathrm{Re}_\tau = 40$, $\mathrm{Wi}_\tau = 310$, $\mathrm{Sc} = 100$ using different spatial resolutions.

on the 4096×768 mesh) is well-converged, and even a 1024×288 mesh provides a relatively accurate solution. For coarser resolutions, the level of turbulent fluctuations starts to rapidly decrease, indicating that the mesh is not able to capture all the relevant scales contributing to the flow dynamics.

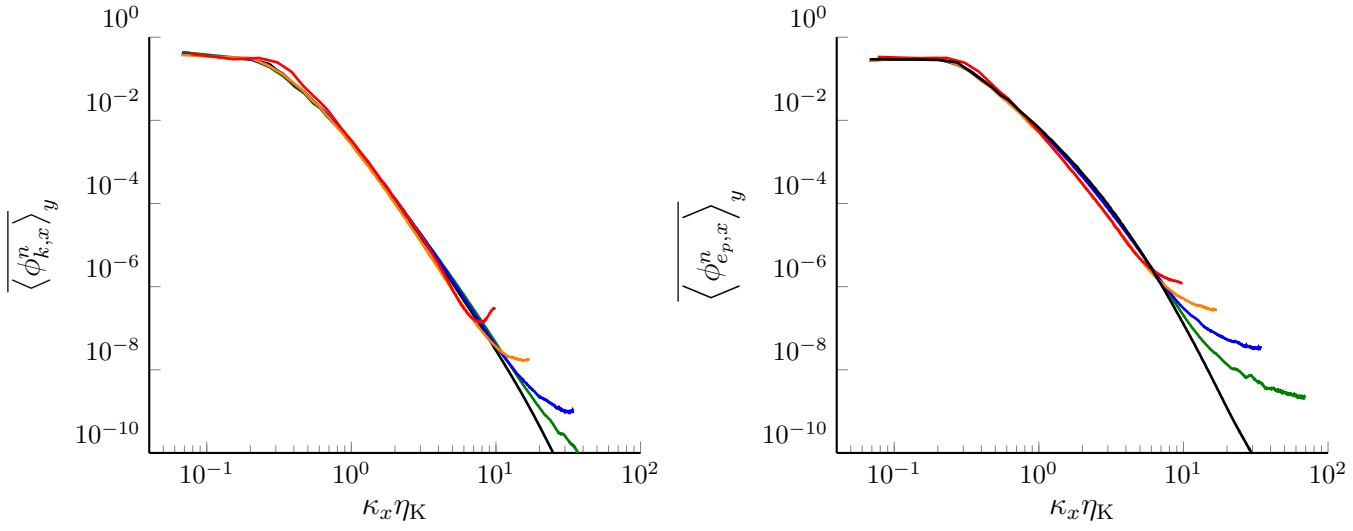

FIG. 3. Wall-normal and time-averaged normalized streamwise spectra of the turbulent kinetic energy k and elastic energy e_p for $\mathrm{Re}_\tau = 40$, $\mathrm{Wi}_\tau = 310$, $\mathrm{Sc} = 100$ on meshes with 256×104, 512×192, 1024×288, 2048×384 and 4096×768 grid points. Wavenumbers are pre-multiplied by the computed wall Kolmogorov length scale $\eta_\mathrm{K} = \left(\nu^3/\epsilon_\mathrm{wall}\right)^{1/4}$.

The distribution of fluctuations across spatial scales is analyzed though the wall-normal and time-averaged normalized streamwise spectra of the turbulent kinetic energy k and elastic energy e_p, as shown in Figure 3 for different

mesh sizes. The two normalized spectra are respectively defined as

$$\phi^n_{k,x}(\kappa_x, y, t) = \frac{1}{I_{\phi_k}}\phi_{k,x}(\kappa_x, y, t) \qquad \text{with} \qquad \phi_{k,x}(\kappa_x, y, t) = \frac{1}{2u_\tau^2}\left[\hat{\mathbf{u}}(\kappa_x, y, t)\cdot\hat{\mathbf{u}}^*(\kappa_x, y, t)\right], \tag{3}$$

$$\phi^n_{e_p,x}(\kappa_x, y, t) = \frac{1}{I_{\phi_{e_p}}}\phi_{e_p,x}(\kappa_x, y, t) \qquad \text{with} \qquad \phi_{e_p,x}(\kappa_x, y, t) = \hat{C}'(\kappa_x, y, t)\cdot\hat{C}'^*(\kappa_x, y, t), \tag{4}$$

where $I_{\phi_\bullet}$ is the integral of $\overline{\langle\phi_{\bullet,x}\rangle}_y$ over $-\infty < \kappa_x < \infty$, the hat operator stands for the Fourier transform along the streamwise x-direction, $\hat{\bullet} = \mathcal{F}_x(\bullet)$, and the star superscript denotes the complex conjugate. Although the integrals I_{ϕ_k} and $I_{\phi_{e_p}}$ strongly depend on the discretization as discussed previously, the normalized spectral densities remain remarkably similar on the different meshes. This suggests that the physical mechanism responsible for the creation of turbulence remains mostly unaffected by the mesh discretization. The effect of a poor spatial resolution manifests itself mostly by the global reduction of the turbulent intensity across all scales. It is worth noting that the 1024×288 mesh, i.e., the coarsest discretization still providing a relatively accurate solution, is also the coarsest mesh that properly captures a scale that is $\sqrt{\mathrm{Sc}} = 10$ times smaller than the computed wall Kolmogorov length scale $\eta_\mathrm{K} = \left(\nu^3/\epsilon_\mathrm{wall}\right)^{1/4}$. This suggests that Batchelor theory for passive scalars provides a good estimate of the smallest scales, even for an active scalar like in EIT. Note finally that the computed wall Kolmogorov scale η_K is about three times larger than the viscous length scale δ_ν.

Finally, the diffusive effect of a finite Schmidt number equal to 100 is evaluated by comparison with simulations using $\mathrm{Sc} = \infty$. As zero-diffusion polymers should theoretically lead to infinitely small scales, the effect of the finite grid used in simulations is assessed by considering three different grid resolutions. The normalized turbulent kinetic and elastic energy spectra are shown in Figure 4. It can be observed that the smallest scales for $\mathrm{Sc} = \infty$ on finite

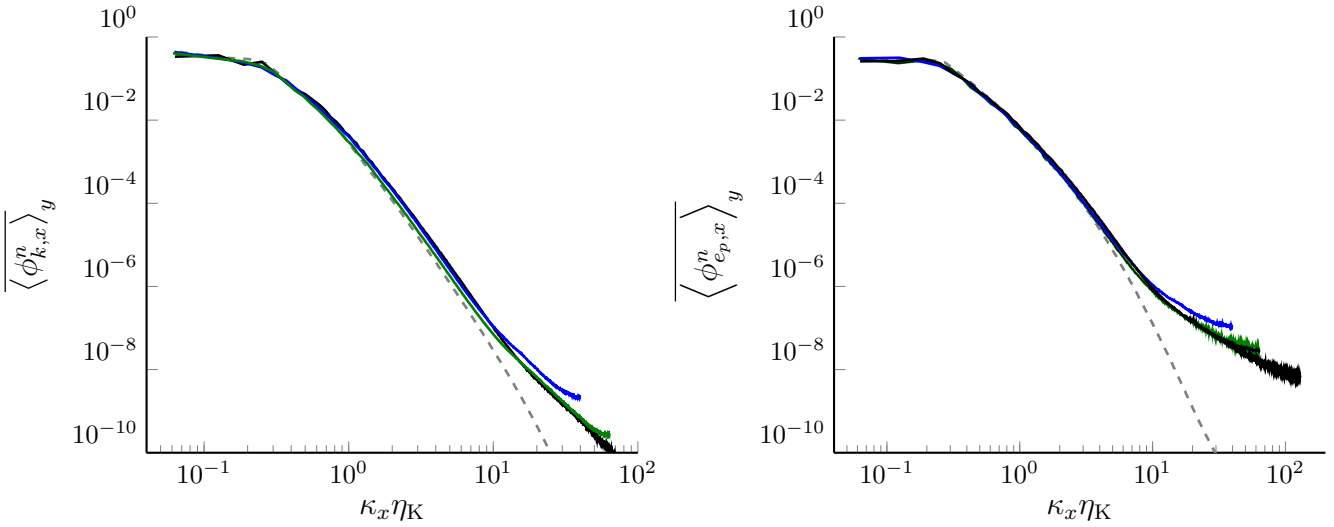

FIG. 4. Wall-normal and time-averaged normalized streamwise spectra of the turbulent kinetic energy k and elastic energy spectra e_p for different discretizations and Schmidt numbers at $\mathrm{Re}_\tau = 40$, $\mathrm{Wi}_\tau = 310$: Sc = 100, 4096×768 (dashed); Sc = ∞, 1280×384; Sc = ∞, 2080×480 and Sc = ∞, 4096×768. Wavenumbers are pre-multiplied by the computed wall Kolmogorov length scale $\eta_\mathrm{K} = \left(\nu^3/\epsilon_\mathrm{wall}\right)^{1/4}$.

meshes are slightly affected by numerical errors, as the diffusive cut-off is not physical but numerical, dictated by the finite size of the smallest grid cells. Part of the energy of the unresolved scales thus piles-up at the end of the spectrum. However, these numerical errors are small and mainly confined at the small scales. Moreover, refining the mesh reduces the impact of these numerical errors. Note that the spectra are here normalized by their respective integrated value. The integrals I_{ϕ_k} and $I_{\phi_{e_p}}$ are therefore reported in table I for the three cases. The amount of turbulent kinetic energy in the flow is larger for $\mathrm{Sc} = \infty$ compared to a finite Schmidt number of 100, indicating that a Schmidt number as large as 10^2 has still a measurable diffusive effect on the solution for the flow conditions considered. Additionally, a finer spatial resolution significantly increases the fluctuations of both the velocity and polymer extension, as a larger portion of the spectrum is captured. This again highlights the importance of small scales in the dynamics of EIT.

The behavior of the solution for $\mathrm{Sc} = \infty$ on grids of finite size results from the dissipation and dispersion introduced by the numerical scheme, similarly to what is observed around shocks in supersonic flows. The adequate grid size is

TABLE I. Turbulent kinetic energy integral I_{ϕ_k} and fluctuating elastic energy integral $I_{\phi_{e_p}}$ for $\mathrm{Re}_\tau = 40$, $\mathrm{Wi}_\tau = 310$.

	$n_x \times n_y$	Sc	I_{ϕ_k}	$I_{\phi_{e_p}}$
A	4096×768	100	$1.53 \cdot 10^{-2}$	$1.05 \cdot 10^{-2}$
B	1280×384	∞	$1.53 \cdot 10^{-2}$	$0.87 \cdot 10^{-2}$
C	2080×480	∞	$1.62 \cdot 10^{-2}$	$0.88 \cdot 10^{-2}$
D	4096×768	∞	$1.68 \cdot 10^{-2}$	$1.04 \cdot 10^{-2}$

thus challenging to estimate *a priori*. This is further illustrated by comparing global flow statistics obtained with two codes using different numerical schemes. The mean profiles of streamwise velocity and polymer elongation are shown in Figure 5 for $\mathrm{Re}_\tau = 85$, $\mathrm{Wi}_\tau = 40$, $\mathrm{Sc} = \infty$. The two codes mainly differ in their discretization of the advective

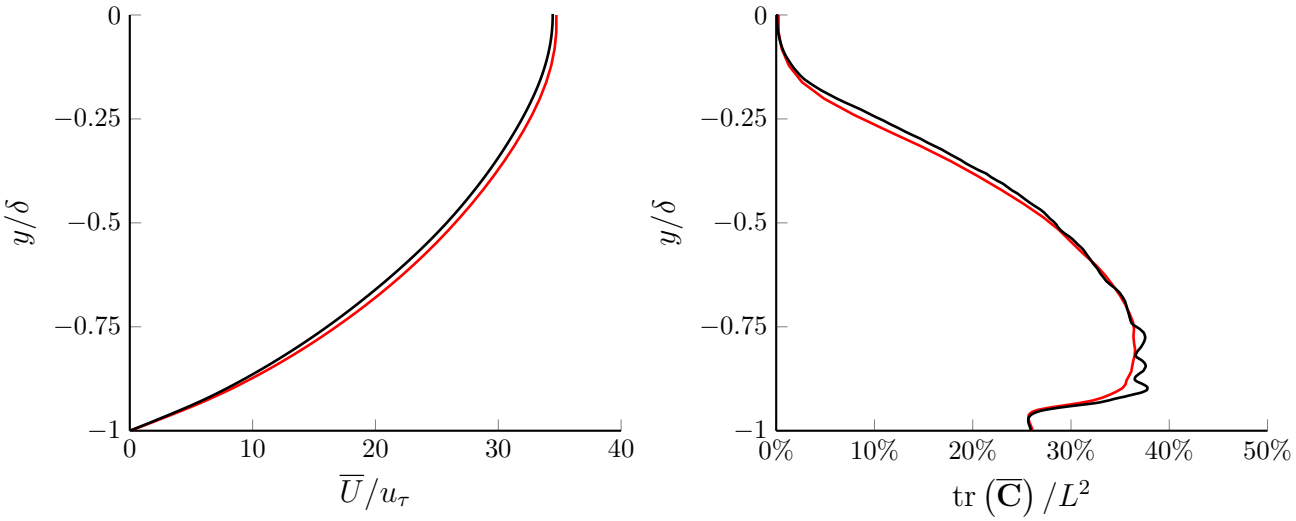

FIG. 5. Mean profiles of the streamwise velocity (left) and polymer elongation (right) for $\mathrm{Re}_\tau = 85$, $\mathrm{Wi}_\tau = 40$, $\mathrm{Sc} = \infty$. The black profiles are obtained with code A using a mesh with 1024×288 grid points whereas the red profiles are obtained with code B using a mesh with 512×128 grid points.

term $\mathbf{u} \cdot \nabla \mathbf{C}$ in the conformation tensor transport equation. This term is critical, as it is responsible for the creation of small elastic scales that are necessary to sustain elasto-inertial turbulence. Code A features a third-order WENO scalar interpolation on a staggered grid, while code B relies on a fourth-order compact interpolation scheme on a collocated grid. Because the third-order WENO scheme is more dissipative, code A requires a finer mesh than code B for converged results, as shown in Figure 5. Nonetheless, if an adequate grid resolution is used, both codes lead to the same mean profiles.

Overall, this supplementary material demonstrates that:

- the critical Schmidt number below which the flow becomes laminar depends on the flow conditions; in particular, elasto-inertial turbulence at larger Reynolds number remains turbulent for lower Schmidt numbers;
- the Batchelor length scale $\eta_\mathrm{B} = \eta_\mathrm{K} \mathrm{Sc}^{-1/2}$ is a good estimation of the smallest elastic scale for finite Schmidt numbers;
- a poor spatial resolution reduces the turbulence intensity in the flow but does not significantly modify its dynamical behaviour;
- the flow solution obtained using zero-diffusion polymers ($\mathrm{Sc} = \infty$) converges as the spatial resolution is increased;
- the discretization necessary to obtain an accurate solution for $\mathrm{Sc} = \infty$ depends on the flow conditions and on the numerical schemes.

These conclusions suggest that the important observations described in the main article are not artefacts of the numerical approach, but indeed represent the actual physics of such flows.